LASER PROPAGATION TEMPORAL SPECTRA

G. W. Reinhardt, et al

Ohio State University

Prepared for:

Advanced Research Projects Agency
Rome Air Development Center

February 1973

RADC-TR-73-66
Technical Report
February 1973

LASER PROPAGATION TEMPORAL SPECTRA

(3432-2)

The Ohio State University

ElectroScience Laboratory

Department of Electrical Engineering
Columbus, Ohio 43212

Sponsored by
Defense Advanced Research Projects Agency
ARPA Order No. 1279

Approved for public release;
distribution unlimited.

Rome Air Development Center
Air Force Systems Command
Griffiss Air Force Base, New York

40R

LASER PROPAGATION TEMPORAL SPECTRA

G. W. Reinhardt
S. A. Collins, Jr.

Contractor: Ohio State University
Contract Number: F30602-72-C-0305
Effective Date of Contract: 1 April 1972
Contract Expiration Date: 31 March 1973
Amount of Contract: $75,000.00
Program Code Number: 9E20

Principal Investigator: Dr. Stuart A. Collins, Jr.
Phone: 614 422-5054

Project Engineer: Edward K. Damon
Phone: 614 422-5953

Contract Engineer: Raymond P. Urtz, Jr.
Phone: 315 330-3443

This research was supported by the Advanced Research Projects Agency of the Department of Defense and was monitored by Raymond P. Urtz, Jr. RADC (OCSE), GAFB, NY 13441 under Contract F30602-72-C-0305.

I-a

UNCLASSIFIED
Security Classification

DOCUMENT CONTROL DATA - R&D

(Security classification of title, body of abstract and indexing annotation must be entered when the overall report is classified)

1. ORIGINATING ACTIVITY *(Corporate author)* ElectroScience Laboratory Department of Electrical Engineering, The Ohio State University, Columbus, Ohio 43212	2a. REPORT SECURITY CLASSIFICATION Unclassified 2b. GROUP

3. REPORT TITLE

LASER PROPAGATION TEMPORAL SPECTRA

4. DESCRIPTIVE NOTES *(Type of report and inclusive dates)*

Technical Report

5. AUTHOR(S) *(Last name, first name, initial)*

Reinhardt, G.W., Collins, S.A., Jr.

6. REPORT DATE	7a. TOTAL NO. OF PAGES	7b. NO. OF REFS
February 1973	~~34~~ 40	4

8a. CONTRACT OR GRANT NO.	9a. ORIGINATOR'S REPORT NUMBER(S)
F30602-72-C-0305 b. ARPA Order No. 1279 c. TASK d.	ElectroScience Laboratory 3432-2 9b. OTHER REPORT NO(S) *(Any other numbers that may be assigned this report)* RADC-TR-73-66

10. AVAILABILITY/LIMITATION NOTICES

Approved for public release; distribution unlimited.

11. SUPPLEMENTARY NOTES	12. SPONSORING MILITARY ACTIVITY
Monitored by Raymond P. Urtz, Jr. RADC (OCSE), GAFB, NY 13441 AC 315 330-3145	Defense Advanced Research Projects Agency Washington, D.C. 22209

13. ABSTRACT

This is a technical report under Contract F30602-72-C-0305 titled "Investigation of Laser Propagation Phenomena," and is a detailed development of the temporal spectra of phase difference fluctuations of atmospherically degraded spherical waves. Some of the results described are summarized in the first quarterly technical report RF 3432-1.

The temporal spectra if for the case of a horizontal wind transverse to the optical path but with points orientated so that their separation vector makes an arbitrary angle with the horizontal. The index of refraction spectrum includes outer-scale effects and allows for other than -11/3 power dependence of the inertial subrange portion of the index of refraction spectrum. The general case results are derived, and then, simplified and presented in detail for the well known Von Karmen Index of Refraction Spectrum.

DD FORM 1 JAN 64 1473

UNCLASSIFIED
Security Classification

I-b

PUBLICATION REVIEW

This technical report has been reviewed and is approved

Raymond P. Utz

RADC Project Engineer

CONTENTS

LASER PROPAGATION TEMPORAL SPECTRA

I. INTRODUCTION

This is a technical report under Contract F30602-72-C-0305 titled "Investigation of Laser Propagation Phenomena". This effort is aimed at providing theoretical support to the RADC Laser Propagation Program in the areas of atmospheric propagation phenomena and microturbulence statistics. The efforts in this report are in support of the experimental program being conducted at RADC. The immediate aim is to give a detailed derivation of the temporal spectrum of phase difference fluctuations.

The work on temporal spectra is of interest because it provides information on time scales of phase and arrival angle useful to systems designers, and further phase difference fluctuations are intimately related to angle of arrival fluctuations for small apertures [Zintsmaster, 1971].

More generally temporal spectral measurements provide a simple method for manipulating experimental data to give a check on our knowledge of the light-beam turbulence interaction. It is much easier to instrument time-spectral measurements because data need be taken for only one apparatus setting. The corresponding spatial correlations or spatial spectra require measurements with apparatus adjusted for many point separations.

Temporal correlations and spectra are in themselves useful quantities to compare with theoretical estimates to gain information about atmospheric-turbulence parameters. In this context, they do not suffer from aperture limitations, as do spatial measurements, because readily available time lags are large enough to represent spatial separations much larger than those conveniently available. Thus they provide a convenient optical means with which to examine outer-scale effects, which are important in the low temporal frequency region of the phase difference spectrum. Further we will show that the high temporal frequency dependence of the phase difference spectrum is easily related to the small separation dependence of the phase structure function, thus allowing a convenient experimental check of $D_S(\rho)$.

The calculation will be done in three steps. In the first step the definition of time lagged phase difference spectra is written in terms of the phase structure function using Taylor's frozen turbulence hypothesis. The result is in terms of a multidimensional integral in rectangular coordinate variables whose integrand includes a generalized isotropic Von Karmen index spectrum. The second step involves evaluating for large and small frequencies all of the indicated integrations except the range integration to obtain the differential

path contribution. The result is put in terms of convenient nondimensional variables. The third step is to perform the range integration for large and small normalized nondimensional temporal frequencies and thereby obtain limiting forms for the complete solution. These forms are tabulated for the generalized index of refraction spectrum and for the usual $\kappa^{-11/3}$ high spatial frequency dependence. The complete solution is obtained for $\kappa^{-11/3}$ inertial subrange dependence by numerical integration for several normalized separations of interest.

II. DERIVATION

The experimental situation is shown in Fig. 1, where a wind of

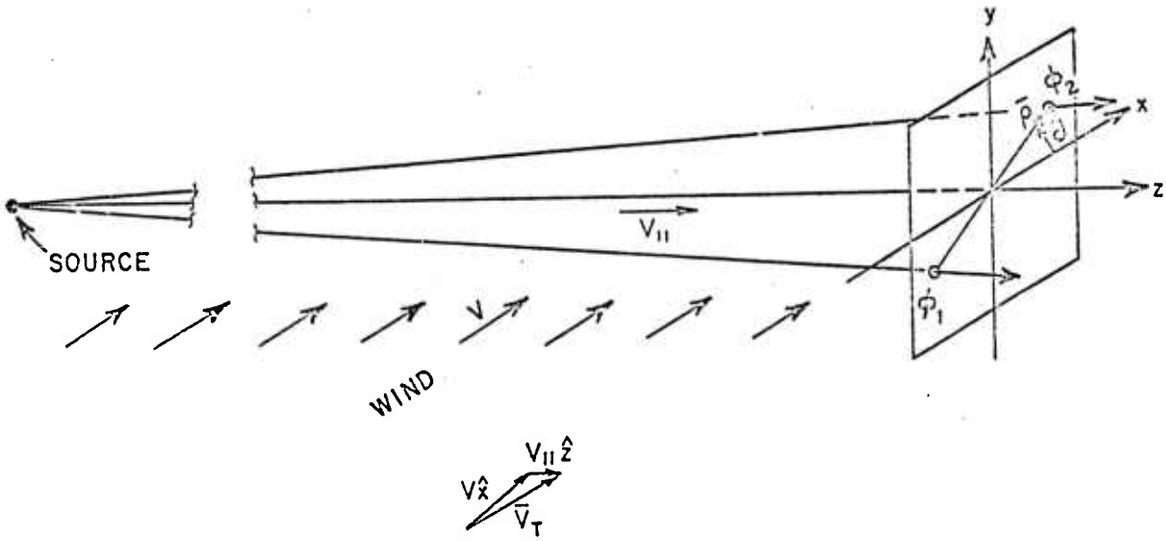

Fig. 1. Diagram of the experimental measurement.

constant velocity $\bar{V}_T$ is blowing. The spherically diverging beam is centered on the z axis. The +x direction is defined so that

$$\bar{V}_T = V\,\hat{x} + V_{II}\,\hat{z}, \tag{1}$$

where V is the magnitude of the transverse wind and V_{II} is the component of the wind parallel to the propagation path. V_{II} may be either a positive or a negative quantity. The phase difference $(\phi_2-\phi_1)$ of two phase points separated by a distance $\bar{\rho}$ in an x-y plane is recorded as a function of time. The vector distance $\bar{\rho}$ makes an arbitrary angle θ with the +x axis, thus enabling us to determine the Fourier transform (F) of the time lagged phase difference

$$W_{\delta s}(\omega,t) = F\langle(\phi_2(\bar{\rho}_2,\tau+t)-\phi_1(\bar{\rho}_1,\tau+t))\,(\phi_2(\bar{\rho}_2,t)-\phi_1(\bar{\rho}_1,t))\rangle \tag{2}$$

for all relative orientations between the phase points and the transverse component of the wind $(V\hat{x})$.

(3) $$(A-B)(C-D) = \frac{1}{2}[(A-D)^2-(A-C)^2+(B-C)^2-(B-D)^2]$$

in Eq. (2) to obtain

(4) $$W_{\delta s} = \frac{1}{2} F\Big\{<[\phi_2(\bar{\rho}_2,\tau+t)-\phi_1(\bar{\rho}_1,t)]^2-[\phi_2(\bar{\rho}_2,\tau+t)-\phi_2(\bar{\rho}_2,t)] + [\phi_1(\bar{\rho}_1,\tau+t)-\phi_2(\bar{\rho}_2,t)]^2-[\phi_1(\bar{\rho}_1,\tau+t)-\phi_1(\bar{\rho}_1,t)]^2\Big\} .$$

Each term in Eq. (4) may be evaluated in terms of a phase structure function

(5) $$<\left(\phi(\bar{\rho}_i,t_i)-\phi(\bar{\rho}_j,t_j)\right)^2> \equiv D_s(\bar{\rho}_i-\bar{\rho}_j,t_i-t_j).$$

A general expression for the wave structure function ($D_W(\rho)$) is obtained by multiplying Hufnagel's (1964) expression for the square of the index of refraction difference by the wave propagation constant squared (k^2). The results are

(6) $$D_W(\rho) = 2k^2 \int_0^\infty d\xi \int_0^L d_\eta \Big\{D_n[\rho_x \tfrac{\eta}{L},\rho_y \tfrac{\eta}{L},\xi]-D_n[0,0,\xi]\Big\}$$

where ξ is the difference range coordinate, η is the average range coordinate.

The phase structure function varies from equality to one-half the wave structure function value as the range increases. Hence

(7) $$D_s(\rho) = \begin{Bmatrix}0.5\\1.0\end{Bmatrix} D_W(\rho),$$

where $\begin{Bmatrix}0.5\\1.0\end{Bmatrix}$ indicates that the numerical coefficient is between 0.5 and 1.0. Alternatively Eqs. (6) and (7) are derived from the spectral expansion solutions for the wave and phase structure functions in Appendix A.

Using Taylor's frozen turbulence hypothesis

(8) $$D_n(\bar{\rho}_i-\bar{\rho}_j,t_i-t_j) = D_n(\bar{\rho}_i-\bar{\rho}_j-\bar{V}_T(t_i-t_j)).$$

Substituting Eqs. (5), (6), (7) and (8) into Eq. (4) yields

$$(9) \qquad W_{\delta s}(\omega) = F\left[\left\{\begin{matrix}0.5\\1.0\end{matrix}\right\} k^2 \int_0^\infty d\xi \int_0^L d\eta \right.$$

$$D_n\left(\frac{\eta}{L}p_x - V\tau, \frac{\eta}{L}p_y, \xi - V_z\tau\right) + D_n\left(-\frac{\eta}{L}p_x - V\tau, \frac{\eta}{L}p_y, \xi - V_z\tau\right)$$

$$\left. - 2D_n(-V\tau, 0, \xi - V_z\tau)\right]$$

where we assume that the turbulence is stationary so that $W_{\delta s}(\omega)$ is not a function of time origin (t). Equation (9) may be written using the explicit Fourier transform relationship

$$(10) \qquad W_{\delta s}(\omega) = \int_{-\infty}^{\infty} d\tau\, D_s(\tau)\, e^{-j\omega\tau}$$

and in terms of the index of refraction spectrum

$$(11) \qquad D_n(X,Y,Z) = 2\int_{-\infty}^{\infty} d\kappa_x \int_{-\infty}^{\infty} d\kappa_y \int_{-\infty}^{\infty} d\kappa_z \,(1-\cos(\kappa_x X + \kappa_y Y + \kappa_z Z)$$

$$\times \Phi_n(\kappa_x, \kappa_y, \kappa_z).$$

The result is

$$(12) \qquad W_{\delta s}(\omega) = \frac{1}{2}\left\{\begin{matrix}0.5\\1.0\end{matrix}\right\} k^2 \int_{-\infty}^{\infty} d\tau \int_0^L d\eta \int_{-\infty}^{\infty} d\xi \int_{-\infty}^{\infty} d\kappa_x \int_{-\infty}^{\infty} d\kappa_y \int_{-\infty}^{\infty} d\kappa_z$$

$$C_n^2(\eta)\Phi_n^{(0)}(\kappa_x, \kappa_y, \kappa_z)$$

$$\cdot\left[-\exp\left\{j(\kappa_x R_x + \kappa_y R_y + \kappa_z \xi - \varepsilon^+\tau)\right\} - \exp\left\{-j(\kappa_x R_x + \kappa_y R_y + \kappa_z \xi - \varepsilon^-\tau)\right\}\right.$$

$$-\exp\left\{j(-\kappa R_x - \kappa_y R_y + \kappa_z \xi - \varepsilon^+\tau)\right\} - \exp\left\{-j(-\kappa R_x - \kappa_y R_y + \kappa_z \xi - \varepsilon^-\tau)\right\}$$

$$\left. +2\exp\left\{j(\kappa_z \xi - \varepsilon^+\tau)\right\} + 2\exp\left\{-j(\kappa_z \xi - \varepsilon^-\tau)\right\}\right]$$

where the cosine terms have been put in terms of exponentials and where

$$R_x \equiv \rho\frac{\eta}{L}\cos\theta \text{ is the range dependent x component of ray separation}$$

$$R_y \equiv \rho\frac{\eta}{L}\sin\theta \text{ is the range dependent y component of ray separation}$$

$$\varepsilon^{\pm} \equiv \kappa_x V + \kappa_z V_z \pm \omega \ .$$

Equation (12) is the complete expression for the time-delayed phase difference spectrum and hence concludes the first step.

We now perform each of the indicated integrations except that for the average range coordinate η, so as to obtain the differential path contribution to $W_{\delta s}(\omega)$. The ξ integration is easily performed resulting in six delta functions involving κ_z in the remaining integrand. The κ_z integration is performed with the result

$$(13) \qquad W_{\delta s}(\omega) = \begin{Bmatrix} 0.5 \\ 1.0 \end{Bmatrix} \pi k^2 \int_{-\infty}^{\infty} d\tau \int_0^L d\eta \int_{-\infty}^{\infty} d\kappa_x \int_{-\infty}^{\infty} d\kappa_y$$

$$C_n^2 \Phi_n^{(0)}(\kappa_x, \kappa_y, 0)\Big[-\exp\left\{j(\kappa_x R_x + \kappa_y R_y - \varepsilon_x^+ \tau)\right\}$$

$$-\exp\left\{-j(\kappa_x R_x + \kappa_y R_y - \varepsilon_x^- \tau)\right\} - \exp\left\{j(-\kappa_x R_x - \kappa_y R_y - \varepsilon_x^+ \tau)\right\}$$

$$-\exp\left\{-j(-\kappa_x R_x - \kappa_y R_y - \varepsilon_x^- \tau)\right\} + 2\exp\left\{-j\varepsilon_x^+ \tau\right\}$$

$$+2\exp\left\{+j\varepsilon_x^- \tau\right\}\Big]$$

where $\varepsilon_x^{\pm} \equiv \kappa_x V \pm \omega$.

Equation (13) shows that only the transverse wind velocity (V) contributes to the temporal spectrum, which agrees with Tatarski's qualitative analysis. The relatively small end effects, which arrise

when the longitudinal wind (V_z) moves turbulence into and out of the beam at the transmitter and receiver, are insignificant for phase point separation much less than the path length.

The above result is a direct consequence of the often used approximation of extending the $\xi(=z_2-z_1)$ integration limits to $\pm\infty$ in the original derivation of $D_S(\rho)$.

The τ and κ_x integrations are done in a similar manner with the result that

$$(14)\qquad W_{\delta S}(\omega) = 8\begin{Bmatrix}0.5\\1.0\end{Bmatrix}\pi^2 k^2 V^{-1}\int_0^L d\eta \int_{-\infty}^{\infty} d\kappa_y \; C_n^2(\eta)\Phi_n^{(0)}\left(\frac{\omega}{V},\kappa_y,0\right)\left[1-\frac{1}{2}\cos\left\{-\frac{\omega}{V}R_x+\kappa_y R_y\right\}-\frac{1}{2}\cos\left\{\frac{\omega}{V}R_x+\kappa_y R_y\right\}\right]$$

where $\Phi_n^{(0)}$ is even in each of its arguments.

Equation (14) may be put into a convenient form by defining dimensionless variables

$$(15a)\qquad \Omega \equiv \frac{\omega\rho}{V} = \text{normalized frequency,}$$

$$(15b)\qquad R(\eta,\nu) \equiv \frac{B(\nu)\rho}{L_o(\eta)} = \text{normalized separation}$$

$$(15c)\qquad \beta^2(\eta,\nu) \equiv \left(1+\left(\frac{B(\nu)\ V}{\omega L_o(\eta)}\right)^2\right) = 1+\left(\frac{R^2(\eta,\nu)}{\Omega^2}\right) = \text{normalized outer scale.}$$

$$(15d)\qquad u \equiv \frac{\eta}{L} = \text{normalized range.}$$

The ν dependence of the constant $B(\nu)$ is described later in Eq. (17c). In terms of the new variables

$$(16) \qquad W_{\delta s} = 16\begin{Bmatrix}0.5\\1.0\end{Bmatrix}\pi^2 k^2 L V^{-1}\rho^{-1}\Omega \int_0^1 du\, C_n^2(u)\beta(u,\nu)$$

$$\int_0^\infty \kappa\left[1 - \frac{1}{2}\cos([-\cos\theta + \kappa\beta\sin\theta]\Omega u)\right.$$

$$\left. - \frac{1}{2}\cos([\cos\theta + \kappa\beta\sin\theta]\Omega u)\right] \Phi_n^{(0)}\left(\frac{\Omega}{\rho}, \frac{\Omega}{\rho}\beta\kappa, 0\right),$$

where $\kappa \equiv \frac{\kappa_y \rho}{\Omega\beta}$ and the evenness of the κ integration has been used to change the integration range. Equation (16) is quite general because neither the functional dependence of $C_n^2(u)$ where u is the normalized average range coordinate nor the form of $\Phi_n^{(0)}(\kappa_x,\kappa_y,\kappa_z)$ has been specified.

In order to determine the differential path contribution, we now define a generalized index of refraction spectrum

$$(17a) \qquad \Phi_n^{(0)} = A(\nu)\left[\left(\frac{B(\nu)}{L_o(\eta)}\right)^2 + \kappa_x^2 + \kappa_y^2 + \kappa_z^2\right]^{-\frac{\nu+3}{2}}$$

where $L_o(\eta)$ is the range dependent outer-scale, and

$$(17b) \qquad A(\nu) = \left[\frac{8\pi}{\nu(\nu+1)}\,\Gamma(1-\nu)\sin\left[(1-\nu)\frac{\pi}{2}\right]\right]^{-1} \qquad \begin{matrix}0<\nu<1\\1<\nu<2\end{matrix}$$

$$A(1) = 1/(2\pi^2)$$

$$(17c) \qquad B(\nu) = \left[2^{1-\nu}\,\frac{\Gamma\left(\frac{2-\nu}{2}\right)}{\Gamma\left(\frac{\nu+2}{2}\right)}\right]^{-\frac{1}{\nu}}.$$

Equation (17a) is a generalized Von Karmen index spectrum with a high spatial frequency dependence of

$$\left[\kappa_x^2+\kappa_y^2+\kappa_z^2\right]^{-\frac{(\nu+3)}{2}} .$$

The generally used value of ν is $\frac{2}{3}$ for which $A(\frac{2}{3}) = 0.033005$ and $B(\frac{2}{3}) = 1.0710$.

The parameters $A(\nu)$ and $B(\nu)$ are defined so that

$$D_n(r) = \begin{cases} C_n^2\, r^{\nu} & r << L_o \\ C_n^2\, L_o^{\nu} & r >> L_o \end{cases} . \tag{18}$$

Equations (17b) and (17c) are derived from Eq. (17a) and the limiting forms (Eq. (18)) in Appendix B.

We now substitute Eq. (17a) into Eq. (16) and after rearranging terms obtain

$$\frac{W_{\delta s}(\Omega)\left(\frac{V}{\rho}\right)}{8\left\{\begin{matrix}0.5\\1.0\end{matrix}\right\}\pi^{5/2}\left(\frac{\Gamma(\frac{\nu+2}{2})}{\Gamma(\frac{\nu+3}{2})}\right) A(\nu)k^2 L_\rho^{\nu+1}} \tag{19}$$

$$= \left[\frac{\sqrt{\pi}}{2}\frac{\Gamma(\frac{\nu+2}{2})}{\Gamma(\frac{\nu+3}{2})}\right]^{-1} \Omega^{-(\nu+2)} \int_0^1 du\; C_n^2(u)\beta^{-(\nu+2)}(u,\nu)$$

$$\times \int_0^\infty d\kappa\Big[1 - \frac{1}{2}\cos\left([-\cos\theta+\kappa\beta(u,\nu)\sin\theta]\Omega u\right)$$

$$- \frac{1}{2}\cos\left([\cos\theta+\kappa\beta(u,\nu)\sin\theta]\Omega u\right)\Big]$$

$$\times (1+\kappa^2)^{-(\frac{\nu+3}{2})} .$$

When $|(\pm\cos\theta+\beta\sin\theta)\Omega u| \ll 1$ Eq. (19) becomes

$$(20)\quad \frac{W_{\delta s}(\Omega)(\frac{V}{\rho})}{8\left\{\begin{matrix}0.5\\1.0\end{matrix}\right\}\pi^{5/2}\left(\frac{\Gamma(\frac{\nu+2}{2})}{\Gamma(\frac{\nu+3}{2})}\right)A(\nu)k^2L\rho^{\nu+1}} \doteq \left[\frac{\sqrt{\pi}}{2}\frac{\Gamma(\frac{\nu+2}{2})}{\Gamma(\frac{\nu+3}{2})}\right]^{-1}\Omega^{-\nu}\int_0^1 du C_n^2(u)\beta^{-(\nu+2)}(u,\nu)\frac{u^2}{2}$$

$$\int_0^\infty d\kappa[\cos^2\theta+\kappa^2\beta^2(u,\nu)\sin^2\theta][1+\kappa^2]^{-(\frac{\nu+3}{2})}.$$

The κ integration is easily performed giving

$$(21a)\quad \frac{W_{\delta s}(\Omega)(\frac{V}{\rho})}{8\left\{\begin{matrix}0.5\\1.0\end{matrix}\right\}\pi^{5/2}\left(\frac{\Gamma(\frac{\nu+2}{2})}{\Gamma(\frac{\nu+3}{2})}\right)A(\nu)k^2L\rho^{\nu+1}} = \Omega^{-\nu}\int_0^1 du\left[\cos^2\theta+\frac{\beta^2(u,\nu)}{\nu}\sin^2\theta\right]$$

$$C_n^2(u)\beta(u,\nu)^{-(\nu+2)}(\frac{3u^2}{6}),$$

and for a horizontal path

$$(21b)\quad \frac{W_{\delta s}(\Omega)(\frac{V}{\rho})}{8\left\{\begin{matrix}0.5\\1.0\end{matrix}\right\}\pi^{5/2}\left(\frac{\Gamma(\frac{\nu+2}{2})}{\Gamma(\frac{\nu+3}{2})}\right)A(\nu)k^2L\rho^{\nu+1}C_n^2} = (\Omega^2+R^2)^{-(\frac{\nu+2}{2})}$$

$$\times\,[\Omega^2\cos^2\theta+(\frac{\Omega^2+R^2}{\nu})\sin^2\theta]\int_0^1 du\,\frac{3u^2}{6}$$

and

$$(21c)\quad 8\pi^{5/2}\,\frac{\Gamma(4/3)}{\Gamma(11/6)}\,A(2/3) = 4.384.$$

When $|(\pm\cos\theta+\beta\sin\theta)\Omega u| << 1$ Eq. (19) becomes

$$(20)\quad \frac{W_{\delta s}(\Omega)(\frac{V}{\rho})}{8\begin{Bmatrix}0.5\\1.0\end{Bmatrix}\pi^{5/2}\left(\frac{\Gamma(\frac{\nu+2}{2})}{\Gamma(\frac{\nu+3}{2})}\right)A(\nu)k^2L\rho^{\nu+1}} \doteq \left[\frac{\sqrt{\pi}}{2}\frac{\Gamma(\frac{\nu+2}{2})}{\Gamma(\frac{\nu+3}{2})}\right]^{-1}\Omega^{-\nu}\int_0^1 du C_n^2(u)\beta^{-(\nu+2)}(u,\nu)\frac{u^2}{2}$$

$$\int_0^\infty d\kappa[\cos^2\theta+\kappa^2\beta^2(u,\nu)\sin^2\theta][1+\kappa^2]^{-(\frac{\nu+3}{2})}.$$

The κ integration is easily performed giving

$$(21a)\quad \frac{W_{\delta s}(\Omega)(\frac{V}{\rho})}{8\begin{Bmatrix}0.5\\1.0\end{Bmatrix}\pi^{5/2}\left(\frac{\Gamma(\frac{\nu+2}{2})}{\Gamma(\frac{\nu+3}{2})}\right)A(\nu)k^2L\rho^{\nu+1}} = \Omega^{-\nu}\int_0^1 du\left[\cos^2\theta+\frac{\beta^2(u,\nu)}{\nu}\sin^2\theta\right]$$

$$C_n^2(u)\beta(u,\nu)^{-(\nu+2)}(\frac{3u^2}{6}),$$

and for a horizontal path

$$(21b)\quad \frac{W_{\delta s}(\Omega)(\frac{V}{\rho})}{8\begin{Bmatrix}0.5\\1.0\end{Bmatrix}\pi^{5/2}\left(\frac{\Gamma(\frac{\nu+2}{2})}{\Gamma(\frac{\nu+3}{2})}\right)A(\nu)k^2L\rho^{\nu+1}C_n^2} = (\Omega^2+R^2)^{-(\frac{\nu+2}{2})}$$

$$\times[\Omega^2\cos^2\theta+(\frac{\Omega^2+R^2}{\nu})\sin^2\theta]\int_0^1 du\ \frac{3u^2}{6}$$

and

$$(21c)\quad 8\pi^{5/2}\frac{\Gamma(4/3)}{\Gamma(11/6)}A(2/3) = 4.384.$$

Thus, there is a quadratic variation (along with any C_n^2 or $\beta(u,\nu)$ variation) of the differential path contribution to $W_{\delta s}(\Omega)$ with range when Ω is small.

When $|(\cos\theta \pm \beta(u,\nu)\sin\theta)\Omega u| \gg 1$ the cosine terms oscillate rapidly and we replace them by their average value (0). The phase difference spectrum is

$$(22a) \qquad \frac{W_{\delta s}(\Omega)\left(\frac{V}{\rho}\right)}{8\begin{Bmatrix}0.5\\1.0\end{Bmatrix}\pi^{5/2}\left(\frac{\Gamma\left(\frac{\nu+2}{2}\right)}{\Gamma\left(\frac{\nu+3}{2}\right)}\right)A(\nu)k^2L\rho^{\nu+1}} = \Omega^{-(\nu+2)}\int_0^1 du C_n^2(u)\beta^{-(\nu+2)}(u,\nu)$$

and for a horizontal path

$$(22b) \qquad \frac{W_{\delta s}(\Omega)\left(\frac{V}{\rho}\right)}{8\begin{Bmatrix}0.5\\1.0\end{Bmatrix}\pi^{5/2}\left(\frac{\Gamma\left(\frac{\nu+2}{2}\right)}{\Gamma\left(\frac{\nu+3}{2}\right)}\right)A(\nu)k^2L\rho^{\nu+1}C_n^2} = (\Omega^2+R^2)^{-\left(\frac{\nu+2}{2}\right)}\int_0^1 du \quad .$$

Equations (22) show that for large $u\Omega$, the only variation in the differential path contribution is due to $C_n^2(u)$ or $\beta(u,\nu)$. Figure 2 shows the limiting forms and the break point location when the path is horizontal. A typical differential path contribution curve would smoothly pass from the low frequency form to the high frequency form and then oscillate with rapidly decreasing amplitude about the high frequency (constant) amplitude. This completes the second step.

The third step is to integrate Eqs. (21b) and (22b) to obtain the final equations. The resultant equations are tabulated in Table 1, for the generalized index spectrum and in more detail in Tables 2, 3 and 4 for the usual case of $\nu=2/3$. In each of the four tables the spectral amplitude has been multiplied by 2 and the range of ω halved to give $0\leq\omega<\infty$(one sided spectrum). In order to get the complete horizontal path solution for $W_{\delta s}(\omega)$, we change the order of integration in Eq. (19) and, assuming constant C_n^2 and L_o, perform the u integration to obtain

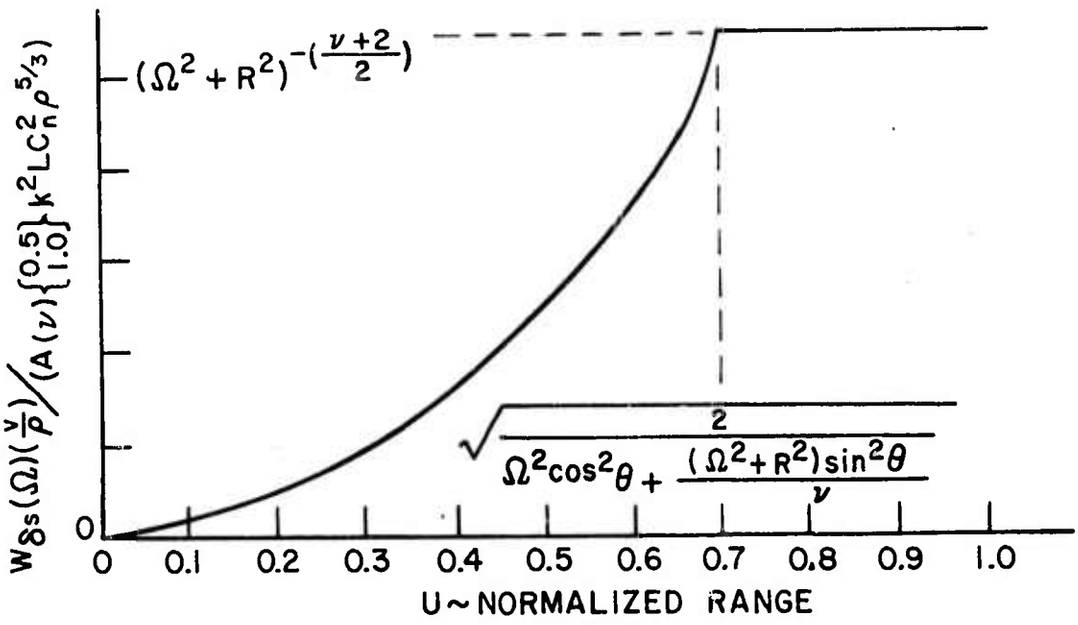

Fig. 2. Differential path contribution limiting forms.

TABLE I

The limiting forms of the one sided phase difference spectrum for any relative orientation (θ) of phase points and wind velocity (V), and for a Von Karmen refractive index spectrum having an index structure function $D_n \approx C_n^2 r^\nu$ when $r << L_o$.

$$\Omega \equiv \frac{2\pi f \rho}{V}, \quad R \equiv \frac{B(\nu)\rho}{L_o} \qquad B(\nu) = \left[2^{-\nu} \frac{(\frac{2-\nu}{2})}{(\frac{\nu+2}{2})} \right]^{-1/\nu} \qquad 0<\nu<2$$

$$A^{-1}(\nu) = \begin{cases} \frac{8\pi}{\nu(\nu+1)} \Gamma(1-\nu)\cos(\nu\frac{\pi}{2}) & 0<|\nu-1|<1 \\ 2\pi^2 & \nu=1 \end{cases}$$

$$\underline{|\pm \cos\theta + (\Omega^2+R^2)^{1/2}\sin\theta| << \sqrt{6}}$$

$$\frac{W_{\delta s}(\Omega)(\frac{V}{\rho})}{16\begin{Bmatrix}0.5\\1.0\end{Bmatrix}\pi^{5/2}\left(\frac{\Gamma(\frac{\nu+2}{2})}{\Gamma(\frac{\nu+3}{2})}\right)A(\nu)k^2 L_\rho{}^{\nu+1}} = \frac{1}{6}(\Omega^2+R^2)^{-(\nu+2)/2}\left[\Omega^2\cos^2\theta + \frac{\Omega^2+R^2}{\nu}\sin^2\theta\right]$$

$$\underline{|\pm\Omega\cos + (\Omega^2+R^2)^{1/2}\sin\theta| >> \sqrt{6}}$$

$$\frac{W_{\delta s}(\Omega)(\frac{V}{\rho})}{16\begin{Bmatrix}0.5\\1.0\end{Bmatrix}\pi^{5/2}\left(\frac{\Gamma(\frac{\nu+2}{2})}{\Gamma(\frac{\nu+3}{2})}\right)A(\nu)k^2 L_\rho{}^{\nu+1}} = (\Omega^2+R^2)^{-(\nu+2)/2}$$

TABLE II

The one sided phase difference spectrum limiting forms for any orientation of phase points and wind velocity

$$\Omega \equiv \frac{2\pi f \rho}{v} \qquad R \equiv \frac{1.071\rho}{L_o} \qquad \nu = 2/3$$

$$\underline{|\pm\Omega\cos + (\Omega^2+R^2)^{1/2}\sin\theta| << \sqrt{6}}$$

$$\frac{W_{\delta s}(\Omega)(\frac{v}{\rho})}{8.77\left\{\begin{matrix}0.5\\1.0\end{matrix}\right\}k^2 L\ C_n^2\rho^{5/3}} = (\Omega^2+R^2)^{-4/3}\left[\frac{\Omega^2\cos^2\theta}{6} + \frac{(\Omega^2+R^2)\sin^2\theta}{4}\right]$$

$$= R^{-8/3}\left[\frac{\Omega^2\cos^2\theta}{6} + \frac{R^2\sin^2\theta}{4}\right], \qquad R >> \Omega$$

$$= \Omega^{-2/3}\left[\frac{\cos^2\theta}{6} + \frac{\sin^2\theta}{4}\right], \qquad \Omega >> R$$

$$\underline{|\pm\Omega\cos + (\Omega^2+R^2)^{1/2}\sin\theta| >> \sqrt{6}}$$

$$= (\Omega^2+R^2)^{-4/3}$$

$$= R^{-8/3} \qquad R >> \Omega$$

$$= \Omega^{-8/3} \qquad \Omega >> R$$

TABLE III

Phase difference spectrum limiting form when the wind direction is parallel to the line connecting the phase points

$$\Omega = \frac{2\pi f \rho}{V} \qquad R = \frac{1.07 l_\rho}{L_o} \qquad \theta = 0^\circ , \quad \nu = 2/3$$

$\underline{R << \sqrt{6}}$

$$\frac{W_{\delta s}(\Omega)\left(\frac{V}{\rho}\right)}{8.77\left\{\begin{matrix}0.5\\1.0\end{matrix}\right\}k^2 L\, C_{n^\rho}^2\, 5/3} = \frac{1}{6} R^{-8/3}\, \Omega^2 \qquad R >> \Omega$$

$$= \frac{1}{6}\, \Omega^{-2/3} \qquad \sqrt{6} >> \Omega >> R$$

$$= \Omega^{-8/3} \qquad \Omega >> \sqrt{6}$$

$\underline{R >> \sqrt{6}}$

$$= \frac{1}{6} R^{-8/3}\, \Omega^2 \qquad 6^{3/14} R^{4/7} >> \Omega$$

$$= \Omega^{-8/3} \qquad \Omega >> 6^{3/14} R^{4/7}$$

TABLE IV

Phase difference spectrum limiting forms when the wind direction is perpendicular to the line connecting the phase point

$$\Omega \equiv \frac{2\pi f \rho}{V} , \qquad R \equiv \frac{1.07 l \rho}{V} , \qquad \theta = 90° , \quad \nu = 2/3$$

$R << \sqrt{6}$

$$\frac{W_{\delta s}(\Omega)\left(\frac{V}{\rho}\right)}{8.77\left[\begin{matrix}0.5\\1.0\end{matrix}\right]k^2 L\, C_{n\rho}^2} = \frac{1}{4} R^{-2/3} \qquad R >> \Omega$$

$$= \frac{1}{4} \Omega^{-2/3} \qquad 2 >> \Omega >> R$$

$$= \Omega^{-8/3} \qquad \Omega >> 2$$

$R >> \sqrt{6}$

$$= R^{-8/3} \qquad R >> \Omega$$

$$= \Omega^{-8/3} \qquad \Omega >> R$$

$$(23)\qquad \frac{W_{\delta s}(\Omega)\left(\frac{V}{\rho}\right)}{8\begin{Bmatrix}0.5\\1.0\end{Bmatrix}\frac{\Gamma\left(\frac{\nu+2}{2}\right)}{\Gamma\left(\frac{\nu+3}{2}\right)}\pi^{5/2}A(\nu)k^2L\rho^{\nu+1}C_n^2} = \left[\frac{\sqrt{\pi}}{2}\,\frac{\Gamma\left(\frac{\nu+2}{2}\right)}{\Gamma\left(\frac{\nu+3}{2}\right)}\right]^{-1}(\Omega\beta)^{-(\nu+2)}$$

$$\times \int_0^\infty d\kappa \left[1 - \frac{1}{2}\,\frac{\sin[\{-\cos\theta+\kappa\beta\sin\theta\}\Omega]}{\{-\cos\theta+\kappa\beta\sin\theta\}\Omega}\right.$$

$$\left. - \frac{1}{2}\,\frac{\sin[\{\cos\theta+\kappa\beta\sin\theta\}\Omega]}{\{\cos\theta+\kappa\beta\sin\theta\}\Omega}\right]\left[1+\kappa^2\right]^{-\left(\frac{\nu+3}{2}\right)} .$$

The integrand in Eq. (23) contains the spatial frequency filter functions and the normalized index of refraction spectrum. Figure 3 shows the filter functions for a particular normalized separation (R) and normalized frequency (Ω), and three orientation angles (θ). The normalized index spectrum is also presented. For 0° and 90° the two sinx/x terms combine to yield a single term. The 0° case has a constant amplitude dependent only on Ω. The 90° case filter function is a sinc function, which discriminates against the low index of refraction spatial frequencies. The general θ case filter function is represented by θ=15° which has two 1/2 amplitude sinc functions that are displaced from the origin.

The integral in Eq. (23) is readily found using numerical integration. The zero degree case is easily evaluated because the filter factor is a constant. In this particular case

$$(24)\qquad \frac{W_{\delta s}(\Omega)\left(\frac{V}{\rho}\right)}{8\begin{Bmatrix}0.5\\1.0\end{Bmatrix}\frac{\Gamma\left(\frac{\nu+2}{2}\right)}{\Gamma\left(\frac{\nu+3}{2}\right)}\pi^{5/2}\,A(\nu)k^2L\rho^{\nu+1}C_n^2} = \left[1 - \frac{\sin\Omega}{\Omega}\right]\left[R^2+\Omega^2\right]^{-\left(\frac{\nu+2}{2}\right)} .$$

Figures 4-7 present the computer generated curves for R = 10, 1.0, 0.1, 0.01; for θ = 0°, 5°, 15°, 45°, 90° and ν=2/3. Also included as narrower lines in the figures are the asymptotic limits determined from Table 2 (θ = 0°, 90° can also be obtained from Tables 3 and 4).

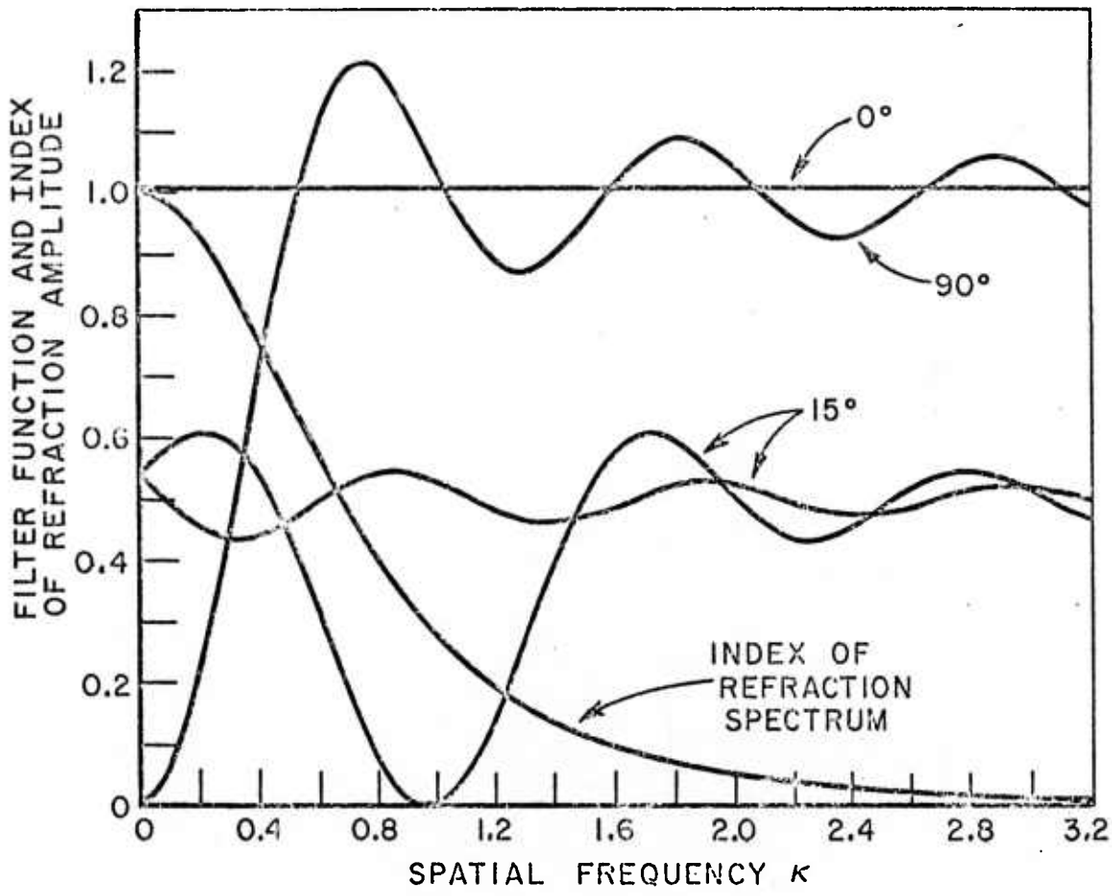

Fig. 3. Examples of the spatial spectral filter functions for various phase point orientations, and the normalized index of refraction spectrum.

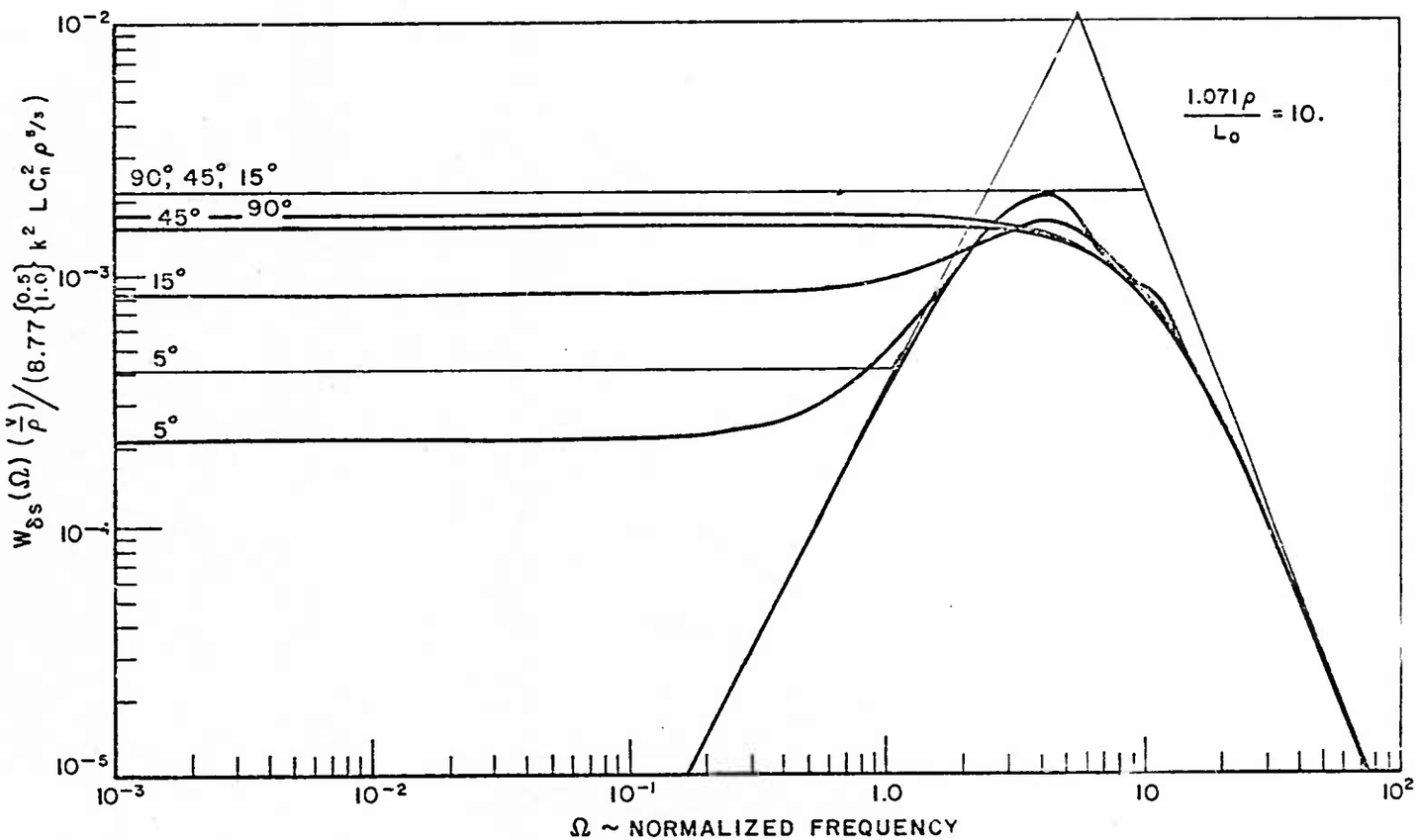

Fig. 4. Normalized phase difference spectrum for a horizontal path versus normalized frequency and orientation angle, when the normalized separation is 10. The light lines are the limiting forms from tables 2, 3 and 4.

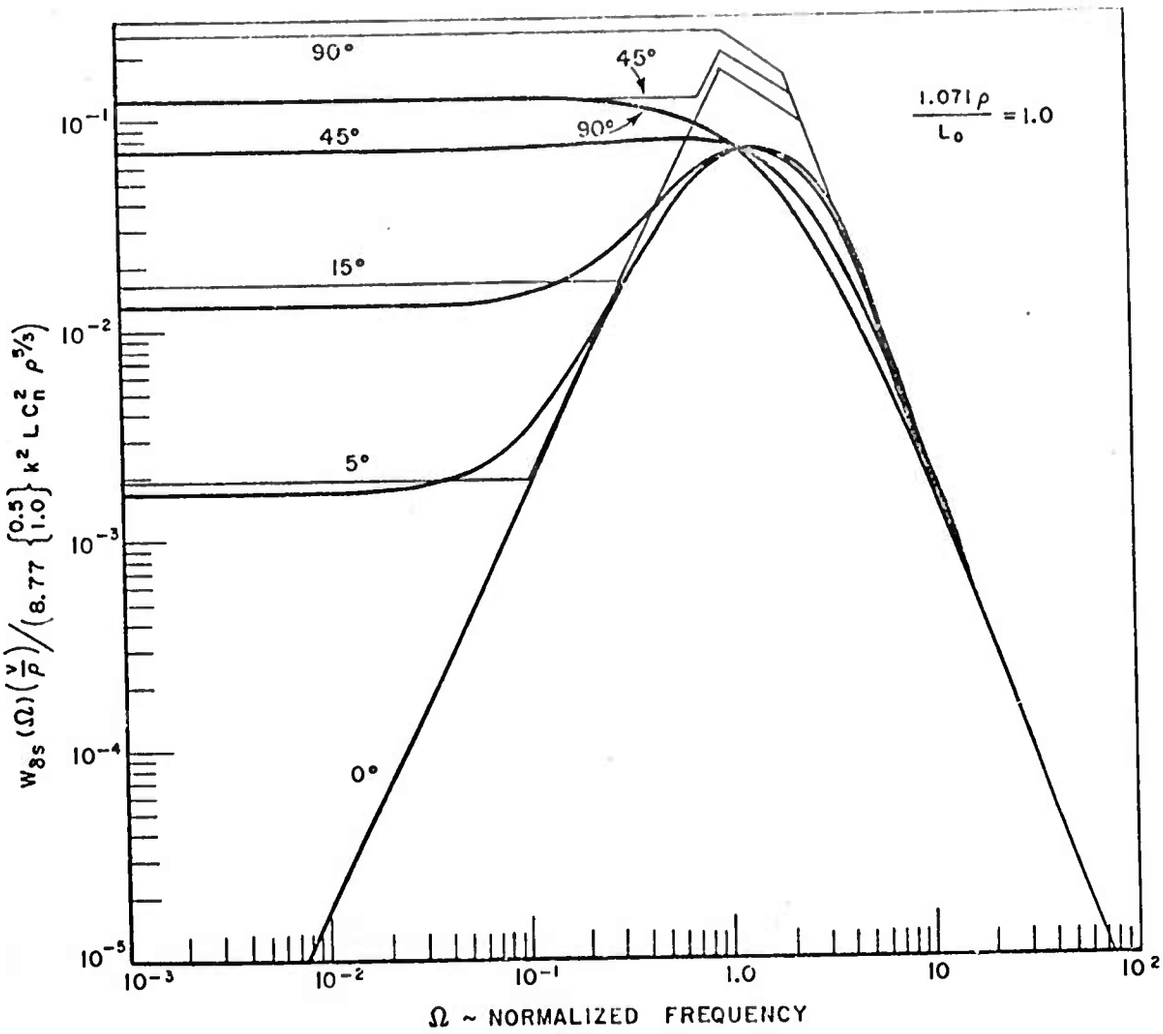

Fig. 5. Normalized phase difference spectrum for a horizontal path versus normalized frequency and orientation angle, when the normalized separation is 1.0. The light lines are the limiting forms from tables 2, 3 and 4.

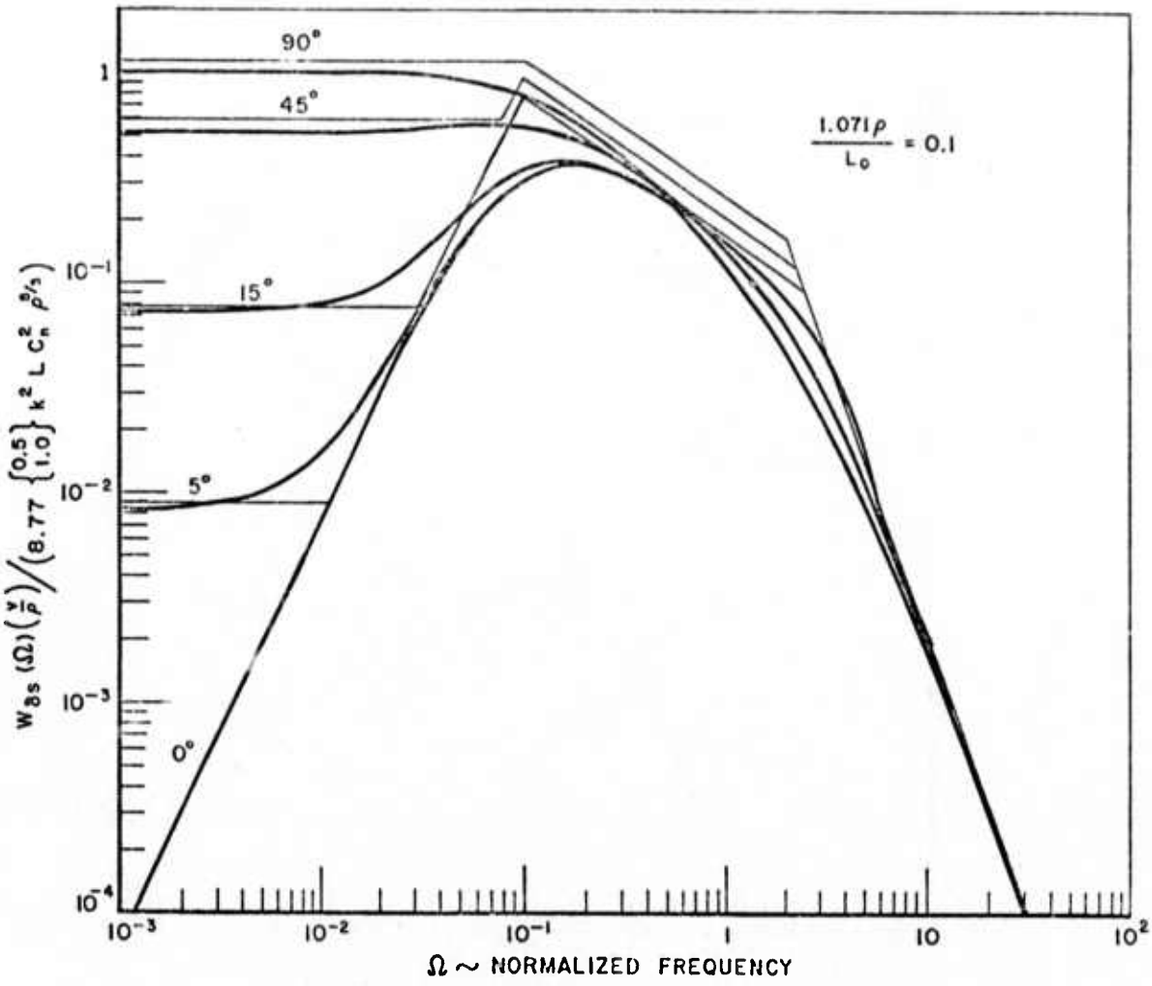

Fig. 6. Normalized phase difference spectrum for a horizontal path versus normalized frequency and orientation angle, when the normalized separation is 0.1. The light lines are the limiting forms from tables 2, 3 and 4.

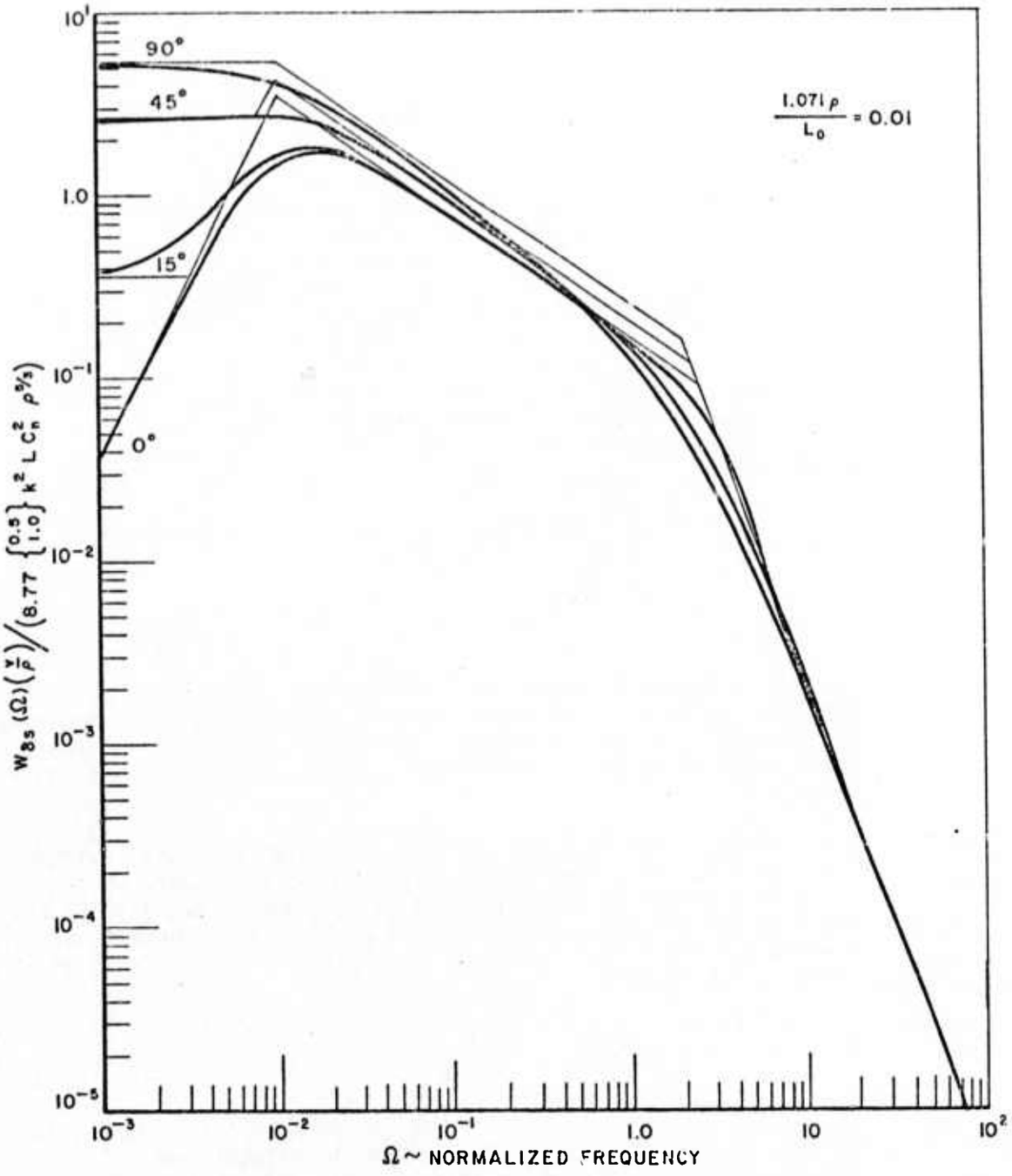

Fig. 7. Normalized phase difference spectrum for a horizontal path versus normalized frequency and orientation angle, when the normalized separation is 0.01. The light lines are the limiting forms from tables 2, 3 and 4.

Figure 4 is for the case

$$R = \frac{1.071\rho}{L_o} = 10$$

which represents a large phase point separation compared to the outer scale. The low frequency offset between the computed curves and low frequency asymptote is due to a higher order term (a constant) that is not included in the low frequency asymptotic solution. An interesting feature of this figure and following Figs. 5, 6 and 7 is that the normalized spectrum approaches a constant level for small normalized frequencies except for the case when the wind is exactly parallel to the phase point separation (θ=0°). A second general result is that the high frequency spectra is independent of orientation angle (θ) and the normalized separation (R), and hence it is also independent of the outer-scale.

It is the mid frequency range that is characterized by the normalized separation. For small

$$R < \begin{cases} \sqrt{6} & \theta = 0° \\ 2 & \theta = 90° \end{cases}$$

the mid frequencies which have a -2/3 slope extend from Ω=R to $\Omega=\sqrt{6}$ for θ=0° and to Ω=2 for θ=90°. Thus for small R, that is phase point separations much less than the outer scale, the lower mid frequency break point determines R and hence L_o since the phase point separation is known.

We may also determine the exponent ν in the phase structure function (Eq. (18)) from phase difference spectrum data by taking the ratio of parallel to perpendicular spectra amplitudes for the case of small normalized separations (R) and small or intermediate normalized frequencies (Ω). From the equations for the limiting forms given in Table 1, the ratio is

$$\left(\frac{\Omega^2}{\Omega^2 + R^2}\right)\nu.$$

This ratio is accurate when $\Omega << R << 1$ or $R << \Omega << 1$ as can be seen in Fig. 7 which shows both the limiting form results and the exact results calculated for the particular value of ν = 2/3. The inequality ($R<<\Omega\leq 1$) defines the more useful Ω range because the ratio

$$\left(\left[\frac{\Omega^2}{R^2+\Omega^2}\right]\nu\right)$$

simplifies to itself. Therefore we have a convenient means of testing the fundamental index of refraction structure function equation which is widely used in turbulence theory (see Eq. (18)).

III. PHYSICAL PICTURE

In order to get a better physical picture of the factors influencing the phase difference temporal spectrum we re-examine several of the previously developed equations.

First put the fundamental definition of the phase difference spectrum given in Eq. (2) in terms of correlation functions,

$$W_{\delta S}(\omega) = \Gamma(2B_S(0,\tau) - B_S(+\rho,\tau) - B_S(-\rho,\tau)). \tag{25}$$

Hence $W_{\delta S}(\omega)$ is the Fourier transform of a combination of four correlation functions. The first two correlations which are combined into one term are between the phase of one ray (see Fig. 1) and the phase of the same ray at a time τ later. This is equivalent to the same time correlation between two parallel rays separated by a distance $v\tau$ arrising from Taylor's frozen turbulence model. The last two terms are phase cross correlations. The cross correlations are between the phase of one ray and the time delayed phase of the other ray. Again using Taylor's frozen turbulence hypothesis the time delay correlation is equivalent to a lateral displacement of the upward ray in a direction opposite to the transverse wind direction. In one case the rays are moved further apart so that they do not cross ($0 \leq z \leq L$) and in the other case they approach each other or cross at a point intermediate to the ray end points.

Now consider the differential path contribution to $W_{\delta S}(\omega)$ from the various terms of Eq. (25), as reflected on the corresponding terms in Eqs. (21b) and (22b). The first term is proportional to range and gives a constant differential path contribution while the last terms have a pronounced range dependent variation due to the range dependent separation between the two rays. Thus the range terms in the differential path contribution to $W_{\delta S}$ increase with range and tend to approach a constant toward the end of the path, thus qualitatively verifying the range dependence of Eqs. (21b) and (22b).

In order to investigate the physical interaction between the refractive index spatial spectrum and the experiment geometry consider the 3-dimensional phase grating model of the atmosphere where each combination of values of κ_x, κ_y and κ_z corresponds to a phase grating with periodic phase variation in the $\bar{\kappa}$ direction. The $\pm z$ directed gratings influence each ray in exactly the same way so they do not contribute to the phase difference and hence the zero for κ_z in Eq. (19) (for example). Hence we consider the gratings which have normals in the x-y plane. Figure 8 further shows two examples

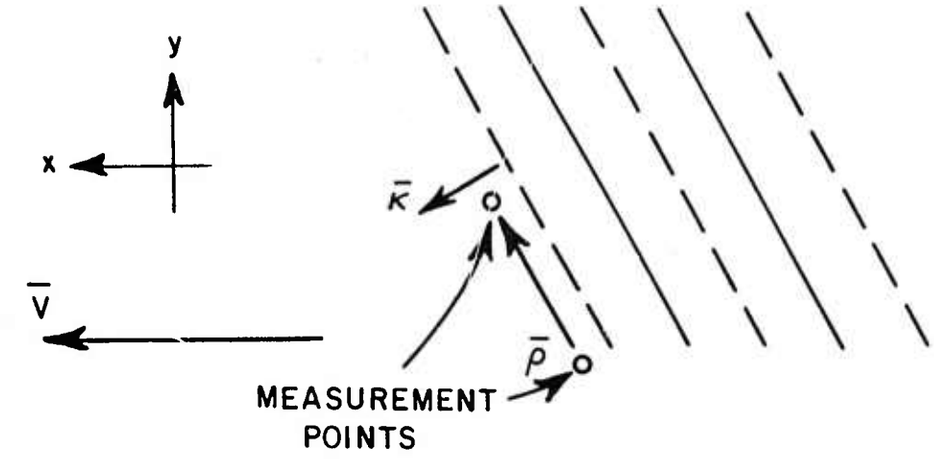

(a)

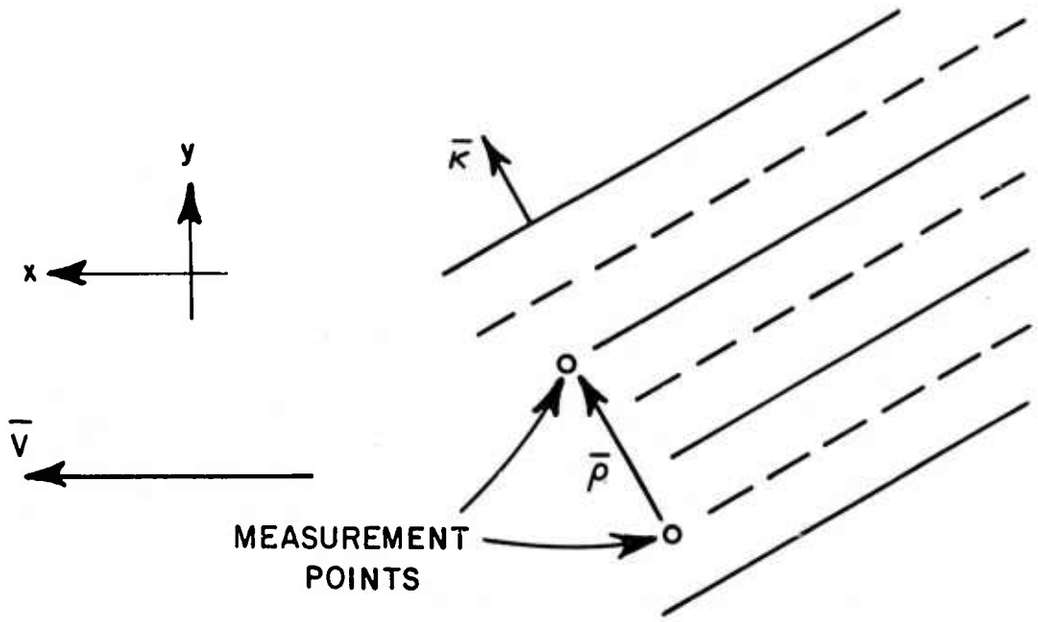

(b)

Fig. 8. Phase grating model of the experimental situation.

of grating orientations (with κ_z=0), that is, gratings with $\bar{\kappa}$ directed perpendicular and parallel to the separations.. The gratings with normals perpendicular to the separation do not influence the phase difference while the parallel case has the maximum effect on the phase difference. Hence the filter function of Eq. (19) has projected the gratings with normal in x-y plane onto the separation vector.

It is the x component of the index spectrum which couples spatial and the temporal frequency variation of the phase difference as the wind moves past the phase points. Hence it is the $\kappa_x = \omega/V$ component that produces the frequency ω in the temporal spectrum. Furthermore, if a particular

$$[\frac{\kappa_x}{n}]$$

(n an integer) which has an associated gratong wavelength, $n\lambda_{\hat{x}}$, that is equal to the local x component of the ray separation (R_x), then the two rays experience identical phase fluctuations and thus zero phase difference at that point on the ray. Hence there is a zero in the differential path contribution to the temporal spectrum at that point. Maxima on the temporal spectrum occur when n is replaced by (n+1/2). This effect is found in Eq. (14), upon expanding the cosine of the sum of two angles and combining terms. These maxima and minima are in the plane wave spectra because there is only one separation for all points on the rays. But the maxima or minima at one point on the spherical wave path is added to the contribution at other points where the filter function is neither at a maxima or a minimum and hence the spherical wave spectra is nearly free of local oscillations in amplitude.

As a final comparison we note that the low temporal frequency spectrum approaches a constant amplitude because of $\omega/V = \kappa_x$ has selected a spatial frequency in the saturation region of the index spectrum. The exception is the 0° case where the filter function has a strong influence. The high frequency temporal spectra goes as

$$(\frac{\omega}{V})^{-(\nu+2)}$$

which results from projecting the $\kappa^{-(\nu+3)}$ index spectrum in the $\bar{\rho}$ direction. This completes the description of salient features of the temporal spectrum in terms of physical concepts.

IV. CONCLUSIONS

The phase difference temporal spectrum has been evaluated for arbitrary orientation of the phase observation points in a plane perpendicular to the beam axis. The calculation has been based on the method of spectral expansions and the Rytov approximation but the equations have been rearranged to emphasize their relationship to the physical picture using a phase screen model. The calculation uses a generalized index of refraction spectrum which has arbitrary power law dependence in the inertial subrange and includes outer-scale effects. This generalization allows one to directly test phase difference spectra measurements to check the generally accepted $\kappa^{-11/3}$ dependence. The development also allows a direct evaluation of the outer-scale.

For a (κ) to the (ν+3) power law inertial subrange spatial frequency dependence, a (κ) to the (ν+2) power law high frequency phase difference temporal spectrum is predicted, independent of phase observation point orientation. The low frequency temporal spectra are strongly orientation dependent. These features are indicated in graphs of typical cases.

BIBLIOGRAPHY

(Zintsmaster, 1971) L.R. Zintsmaster, Angle of Arrival Calculations at 10.6μ, The Ohio State University ElectroScience Laboratory Report 3163-1 (1971).

(Hufnagel, 1964) R.E. Hufnagel, N.R. Stanley, Modulation Transfer Function Associated with Image Transmission Through A Turbulent Media, J. Opt. Soc. Am. 54 (1964) pp. 52-61.

(Tatarski, 1961) V.I. Tatarski, Wave Propagation in a Turbulent Medium, Translated by R.A. Solverman, Dover (1967).

(Carlson, 1969) F.P. Carlson, A. Ishimaru, The Propagation of Spherical Waves in Locally Homogeneous Random Media, J. Opt. Soc. Am. 59 (1969) pp. 319-327.

APPENDIX A

In this appendix we obtain the phase structure function in terms of spatial coordinate integrations from the often used spectral expansion results.

We start the calculation by comparing the spherical wave phase structure function (Carlson, 1969)

$$\text{(A1a)} \qquad D_s(\rho) = 8k^2\pi^2 \int_0^\infty d\kappa\, [1-J_0(\kappa\rho)]\kappa \int_0^L d\eta\, C_n^2(\eta) \left(\frac{L}{\eta}\right)^2$$

$$\cos^2\left(\frac{L(L-\eta)\kappa^2}{2k\eta}\right) \phi_n^{(0)}\left(\frac{\kappa L}{\eta}\right)$$

and the spherical wave, wave structure function

$$\text{(A1b)} \qquad D_w(\rho) = 8k^2\pi^2 \int_0^\infty d\kappa \left(1-J_0(\kappa\rho)\right)\kappa \int_0^L d\eta\, C_n^2(\eta) \left(\frac{L}{\eta}\right)$$

$$\phi_n^{(0)}\left(\frac{\kappa L}{\eta}\right)$$

where

k	is the source wave number
ρ	is the measurement separation
L	is the propagation range
$C_n^2(\eta)$	is the turbulence strength
$\phi_n^{(0)}(\kappa)$	is the turbulence spectrum

and $\kappa = \sqrt{\kappa_x^2 + \kappa_y^2}$.

The phase structure function in Eq. (A1a) is identical to the wave structure function in Eq. (A1b) except that the former has an additional cosine squared term in its integrand. For the case of small separations (ρ) and long ranges (L) the cosine squared term oscillates rapidly during the significant part of the κ integration

and we can replace the cosine squared term by its average value (0.5). When ρ is large and L is small, the cosine squared term remains essentially constant during the significant part of the κ integration and we may replace it by its initial value (1.0). Other values of ρ and L result in an intermediate effective contribution of the cosine squared term to the value of $D_s(\rho)$, hence

$$(A2a) \qquad D_s(\rho) = \begin{Bmatrix} 0.5 \\ 1.0 \end{Bmatrix} D_w(\rho).$$

Using Eqs. (A1b) and (A2a), and setting $\kappa' \equiv \kappa \frac{L}{\eta}$ yields

$$(A2b) \qquad D_s(\rho) = 8k^2\pi^2 \begin{Bmatrix} 0.5 \\ 1.0 \end{Bmatrix} \int_0^L d\eta \; C_n^2(\eta) \int_0^\infty d\kappa' \; \kappa' \left(1-J_o\left(\frac{\eta\kappa'\rho}{L}\right) \phi_n^{(0)}(\kappa')\right) .$$

In all subsequent equations, drop the prime. κ is the magnitude of the spatial frequency in the X-Y plane. We regain the orientation dependence of the spatial frequency by using the identity

$$(A3) \qquad \frac{1}{2\pi} \int_0^2 d\phi \left(1-\cos\left(\frac{\eta\kappa\rho}{L} \cos\phi\right)\right) = 1-J_o\left(\frac{\eta\kappa\rho}{L}\right)$$

where ϕ is the angle between κ and ρ in the X-Y plane. Substituting Eq. (A3) into Eq. (A2) and changing to rectangular coordinates yields

$$(A4) \qquad D_s(\rho) = 4 \begin{Bmatrix} 0.5 \\ 1.0 \end{Bmatrix} \pi k^2 \int_0^L d\eta \; C_n^2(\eta) \int_{-\infty}^\infty d\kappa_x \int_{-\infty}^\infty d\kappa_y \; \phi_n^{(0)}(\kappa_x,\kappa_y,0)\left(1-\cos\left\{\frac{\eta}{L}\left(\kappa_x\rho_x+\kappa_y\rho_y\right)\right\}\right) .$$

The relationship between the three dimensional index of refraction spectrum and the two dimensional spectrum is

$$\text{(A5)} \qquad \Phi_n^{(0)}(\kappa_x,\kappa_y,0) = \frac{1}{2\pi} \int_{-\infty}^{\infty} F(\kappa_x,\kappa_y,|\xi|)\, d\xi,$$

and the relationship between the two dimensional index of refraction spectrum and the index of refraction structure function is

$$\text{(A6)} \qquad 2 \int_{-\infty}^{\infty} d\kappa_x \int_{-\infty}^{\infty} d\kappa_y\, F(\kappa_x\kappa_y,|\xi|)(1-\cos\left\{\left(\frac{\eta}{L}\right)(\kappa_x\rho_x+\kappa_y\rho_y)\right\}$$

$$= D_n\left(\frac{\eta}{L}\rho_x,\frac{\eta}{L}\rho_y,|\xi|\right) - D_n(0,0,|\xi|).$$

Substituting Eqs. (A6) and (A5) into Eq. (A4) yields the required result,

$$\text{(A7)} \qquad D_s(\rho) = \left\{\begin{matrix}0.5\\1.0\end{matrix}\right\} k^2 \int_{-\infty}^{\infty} d\xi \int_0^L d\eta\left(D_n\left(\frac{\eta}{L}\rho_x,\frac{\eta}{L}\rho_y,\xi\right) - D_n(0,0,\xi)\right)$$

where we drop the magnitude sign since we require that D_n be even in each of its three arguments.

APPENDIX B

We will now derive the constants in a generalized isotropic Von Karmen index spectrum such that the corresponding index structure function is

$$(B1) \qquad D_n(r) = \begin{cases} C_n^2 \, r^{\nu} & r << L_o \\ C_n^2 \, L_o^{\nu} & r >> L_o \end{cases}$$

where C_n^2 is the turbulence strength, and L_o is the outer scale.

The inclusion of the parameter ν allows the experimentalist to test the widely used 2/3 power (ν=2/3) variation of D_n with separation (r).

A general expression for the three dimensional isotropic index of refraction spectrum is

$$(B2) \qquad \phi_n(\kappa) = \frac{A(\nu) \, C_n^2}{\left[(B(\nu)/L_o)^2 + \kappa^2\right]^{\frac{\nu+3}{2}}}$$

where the constants $A(\nu)$ and $B(\nu)$ are to be evaluated. The exponent has been chosen such that

$$(B3) \qquad D_n(r) = 2 \int_{-\infty}^{\infty}\int_{-\infty}^{\infty}\int_{-\infty}^{\infty} (1-\cos(\bar{\kappa}\cdot\bar{r})) \, \Phi_n(\bar{\kappa}) \, d\bar{\kappa}$$

The general inverse transform relationship (Tatarski 1961) for isotropic turbulence is

$$(B4) \qquad D_n(r) = 8\pi \int_0^{\infty} \left(1 - \frac{\sin \kappa r}{\kappa r}\right) \phi_n(\kappa) \, \kappa^2 d\kappa.$$

Substitute Eq. (B2) into Eq. (B4) to obtain

$$(B5)\quad D_n(r) = 8\pi\, A(\nu)\, C_n^2 \int_0^\infty \left(1 - \frac{\sin \kappa r}{\kappa r}\right) \frac{\kappa^2}{\left[\left(\frac{B(\nu)}{L_o}\right)^2 + \kappa^2\right]^{\frac{\nu+3}{2}}}\, d\kappa \quad .$$

Then change variables

$$(B6)\qquad \omega = \kappa r$$

and obtain

$$(B7)\qquad D_n(r) = 8\pi\, A(\nu)\, C_n^2\, r^\nu \int_0^\infty \left(1 - \frac{\sin\omega}{\omega}\right) \frac{\omega^2\, d\omega}{\left(\left(\frac{Br}{L_o}\right)^2 + \omega^2\right)^{\frac{\nu+3}{2}}} \quad .$$

When $r/L_o << 1$ we drop the Br/L_o term as being small in comparison to ω during the significant part of the integration, and using Eq. (B1) obtain

$$(B8)\quad A(\nu) = \left[8\pi \int_0^\infty \left(1 - \frac{\sin\omega}{\omega}\right) \omega^{-(\nu+1)}\, d\omega\right]^{-1} \quad .$$

The integration is put into a more tractable form by noting that

$$(B9)\quad \int_0^\infty \left(1 - \frac{\sin\omega}{\omega}\right) \omega^{-(\nu+1)} d\omega =$$

$$\int_0^\infty d\omega \int_0^1 da \int_0^a db\, \sin(b\omega)\, \omega^{-\nu} \quad .$$

Equation (B9) is easily evaluated when $\nu = 1$, the result being $\pi/4$. When $\nu \neq 1$, interchange integration limits and using

$$(B10) \qquad \int_0^\infty \sin(\omega)\, \omega^{-\nu}\, d\omega = \Gamma(1-\nu)\sin\left[(1-\nu)\,\frac{\pi}{2}\right]$$

to obtain $A(\nu)$ when $0 < |\nu-1| < 1$. The final result for $A(\nu)$ is

$$(B11) \qquad A(\nu) = \left[\frac{8\pi}{\nu(\nu+1)}\,\Gamma(1-\nu)\sin(1-\nu)\,\frac{\pi}{2}\right]^{-1} \qquad 0 < \nu < 1$$

$$1 < \nu < 2$$

$$= \frac{1}{2\pi^2} \qquad \nu = 1$$

When $U \equiv \kappa/B$ is substituted into Eq. (5) the result is

$$(B12) \qquad D_n(r) = 8\pi C_n^2 A(\nu) \left(\frac{B(\nu)}{L_o}\right)^{\nu}$$

$$* \int_0^\infty \left[1 - \frac{\sin\left(u\,\frac{rB}{L_o}\right)}{\left(u\,\frac{rB}{L_o}\right)}\right] \frac{u^2 du}{(1+u^2)^{(\nu+3)/2}} \,.$$

When $rB/L_o >> 1$ we may neglect the sine term and easily integrate to obtain an expression involving the remaining constant $B(\nu)$. Using Eq. (B1)

$$(B13) \qquad B(\nu) = [4\pi\, B(3/2,\, \nu/2)\, A(\nu)]^{\nu} \,.$$

Upon substituting Eq. (B11) into Eq. (B13) we obtain the final expression for $B(\nu)$.

$$(B14) \qquad B(\nu) = \left[2^{(1-\nu)}\,\frac{\Gamma(\frac{2-\nu}{2})}{\Gamma(\frac{\nu+2}{2})}\right]^{-\frac{1}{\nu}}$$

The complete expression for the phase structure function is

$$(B15) \qquad D_n(r) = C_n^2 L_o^{\nu} \left(1 - \Gamma(\nu/2) 2^{\left(\frac{\nu-2}{2}\right)} \left(\frac{rB(\nu)}{L_o} \right)^{\nu/2} K_{\nu/2} \left(\frac{rB(\nu)}{L_o} \right) \right)$$

where we have used Tatarski's (1961) transform pair.